Insights into HO_X and RO_X chemistry in the boreal forest via measurement of peroxyacetic acid, peroxyacetic nitric anhydride (PAN) and hydrogen peroxide

John N. Crowley[1], Nicolas Pouvesle[1], Gavin J. Phillips[1], Raoul Axinte[1], Horst Fischer[1], Tuukka Petäjä[2], Anke Nölscher[1], Jonathan Williams[1], Korbinian Hens[1], Hartwig Harder,[1] Monica Martinez-Harder[1], Anna Novelli[1], Dagmar Kubistin[1], Birger Bohn[3], and Jos Lelieveld[1].

[1]**Division of Atmospheric Chemistry, Max-Planck-Institute für Chemie, Mainz, Germany**
[2]**Institute for Atmospheric and Earth System Research INAR / Physics, University of Helsinki, Finland**
[3]**Forschungszentrum Juelich GmbH, 52425 Juelich, Germany**

Correspondence to: John N. Crowley (john.crowley@mpic.de)

Supplementary Information

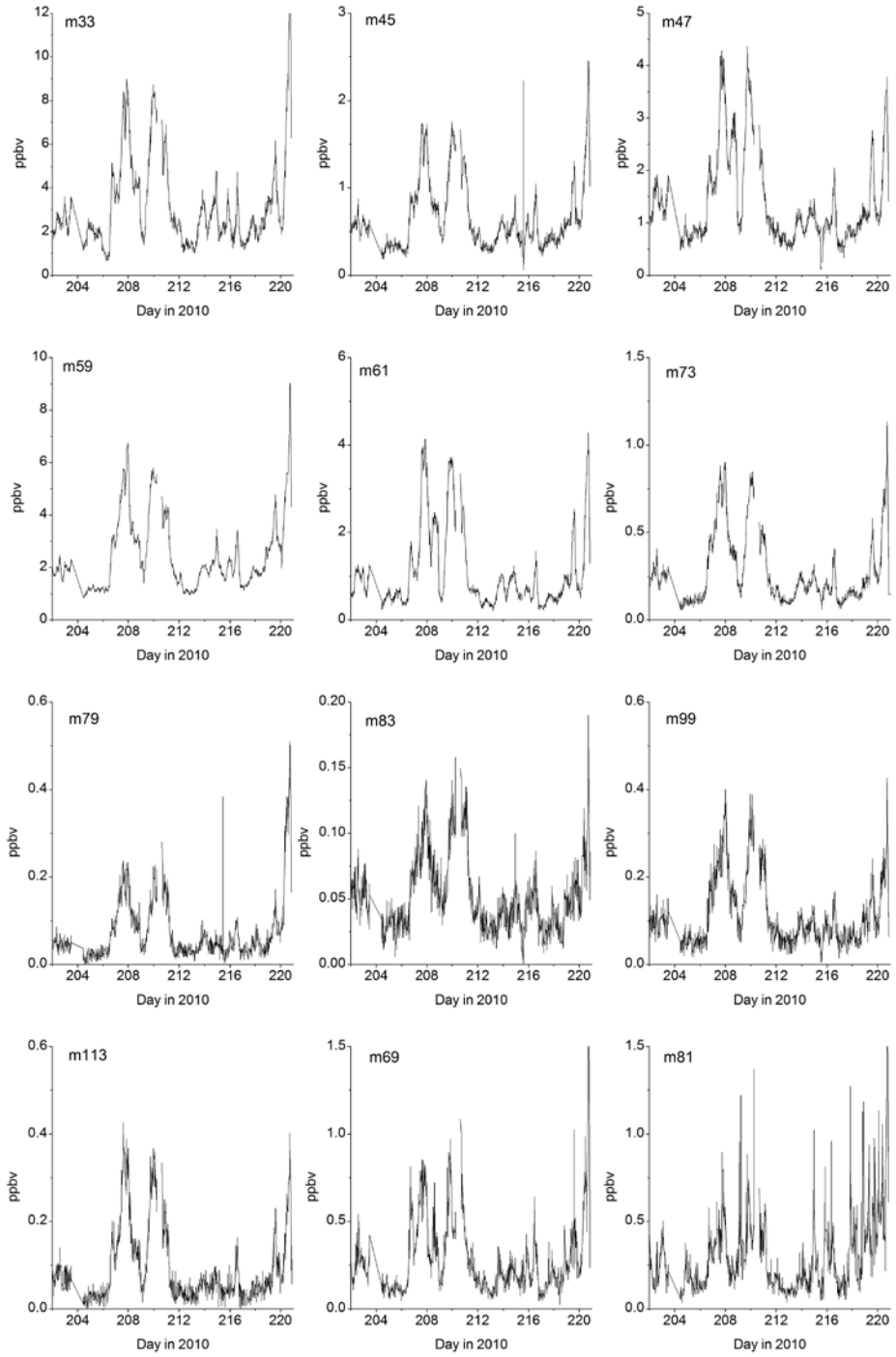

Figure S1. Selected PTRMS masses observed during the HUMPPA-COPEC campaign.

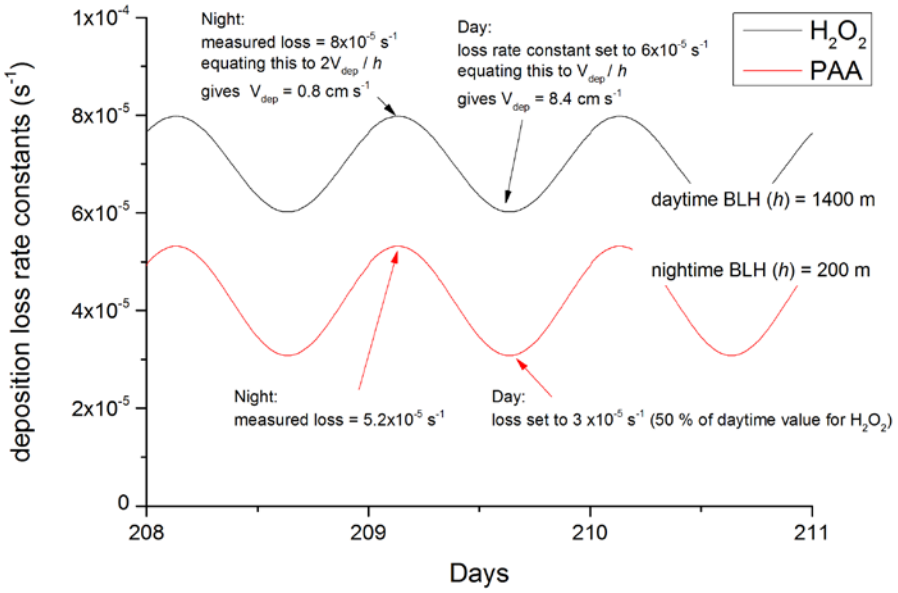

Figure S2. Campaign deposition velocities for PAA and H_2O_2.

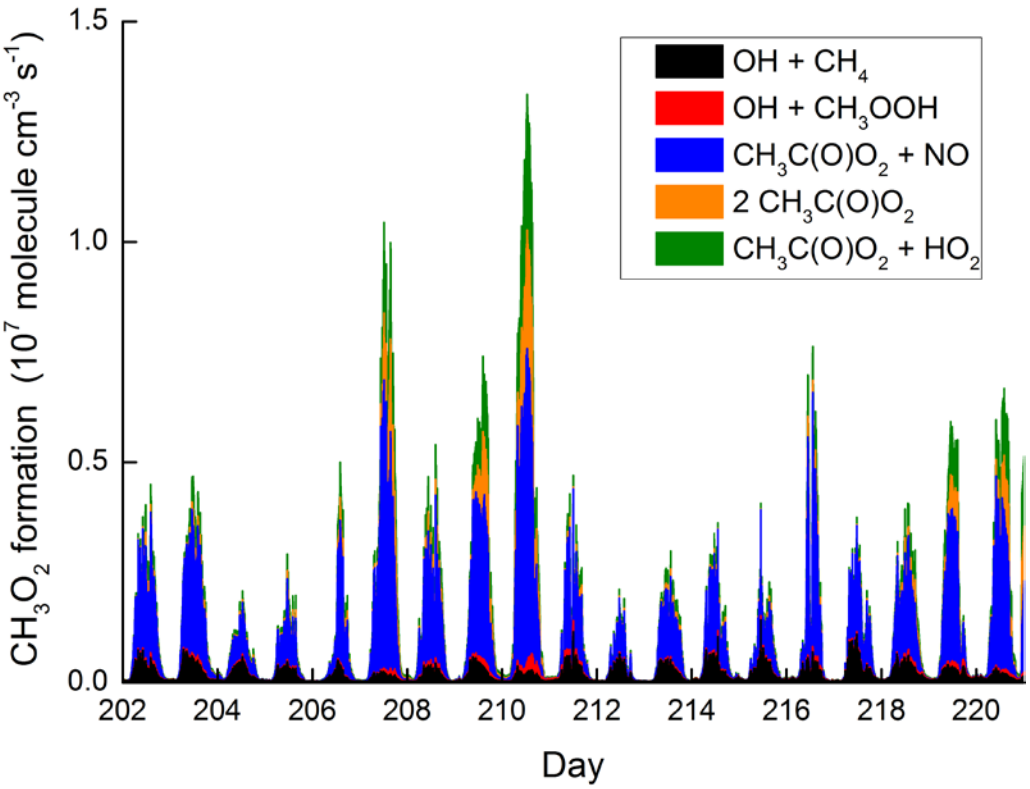

Figure S3. Modelled flux (molecule cm^{-3} s^{-1}) through reactions that lead to CH_3O_2 formation.

Table S1. Reactions used in the box-model.

Reaction / Process	Rate constant [a]	Reference / comment
Formation of OH and HO_2		
$O_3 \rightarrow 2\ OH$	J-O(^{1}D)	b
$HONO \rightarrow OH + NO$	J-NO_2 × 0.165	
$HCHO \rightarrow 2\ HO_2$	J-HCHO	c
$HC(O)CHO + h\nu \rightarrow 2\ HO_2$	J-NO_2 × 0.0076	
$HO_2 + NO \rightarrow NO_2 + OH$	3.45×10^{-12}exp(270/T)	
$HO_2 + O_3 \rightarrow OH$	2.03×10^{-16}(T/300)$^{4.57}$exp(693/T)	
O_3 + terpenes $\rightarrow$ OH	2.0×10^{-16} * 0.8	
$OH + CO \rightarrow HO_2$	1.44×10^{-13} (1+M/4.2× 10^{19})	
$OH + HCHO \rightarrow HO_2$	5.4×10^{-12} exp(135/T)	
$OH + O_3 \rightarrow HO_2$	1.7×10^{-12}exp(-940/T)	
$OH + CH_4 + O_2 \rightarrow CH_3O_2$	1.85×10^{-12} exp(-1690/T)	
$CH_3O_2 + NO \rightarrow HO_2 + NO_2 + HCHO$	2.3×10^{-12} exp(360/T)	
$RO_2 + NO \rightarrow HO_2$	1×10^{-11}	
$RO_2 + HO_2 \rightarrow ROOH$	8×10^{-12}	
$RO_2 + HO_2 \rightarrow OH$	2×10^{-12}	
$RO_2 + RO_2 \rightarrow 2\ HO_2$	1×10^{-12}	
Formation of $CH_3C(O)O_2$ and RO_2		
$OH + CH_3CHO \rightarrow CH_3C(O)O_2$	4.7×10^{-12}exp(345/T)	
$CH_3C(O)CHO + h\nu \rightarrow CH_3C(O)O_2 + HO_2$	J-NO_2 × 0.019	
$CH_3C(O)C(O)CH_3 + h\nu \rightarrow 2\ CH_3C(O)O_2$	J-NO_2 × 0.208	
$CH_3C(O)C(O)OH + h\nu \rightarrow CH_3C(O)O_2 + HO_2$	J-NO_2 × 0.033	
$OH + OVOC + O_2 \rightarrow RO_2 + H_2O$	1×10^{-11}	
OH + terpenes (O_2) $\rightarrow$ RO_2	7×10^{-11}	
Formation of PAN, PAA and H_2O_2		
O_3 + terpenes $\rightarrow$ H_2O_2	2.0×10^{-16} * 0.17	
$CH_3C(O)O_2 + NO_2 \rightarrow PAN$	T and P dependent	
$CH_3C(O)O_2 + HO_2 \rightarrow PAA + O_2$	3.14×10^{-13}*exp(580/T) × 0.37	
$CH_3C(O)O_2 + HO_2 \rightarrow CH_3C(O)OH + O_3$	3.14×10^{-13}*exp(580/T) × 0.13	
$CH_3C(O)O_2 + HO_2 \rightarrow OH$	3.14×10^{-13}*exp(580/T) × 0.50	
$HO_2 + HO_2 \rightarrow H_2O_2 + O_2$	(T, P, H_2O) dependent	
Loss of PAN and PAA and H_2O_2		
$OH + PAA \rightarrow CH_3C(O)O_2 + H_2O$	1×10^{-11}	
$PAN \rightarrow CH_3C(O)O_2 + NO_2$	T and P dependent	
$CH_3C(O)O_2 + NO \rightarrow NO_2 + CH_3O_2 + CO_2$	7.5e-12*exp(290/T)	
$H_2O_2 + OH \rightarrow HO_2 + H_2O$	2.9e-12*exp(-160/T)	
$H_2O_2 + h\nu \rightarrow OH + OH$	J-H_2O_2	
Other reactions		
$NO_2 \rightarrow NO + O_3$	J-NO_2	d
$NO + O_3 \rightarrow NO_2$	3.0e-12*exp(-1500/T)	d
$OH + NO_2 \rightarrow HNO_3$	T and P dependent	
$CH_3O_2 + HO_2 \rightarrow CH_3OOH$	$3.8x\ 10^{-13}$ exp(780/T)	
$OH + CH_3OOH \rightarrow CH_3O_2 + H_2O$	0.6 * 5.3e-12exp(190/T)	
$OH + CH_3OOH \rightarrow HCHO + OH + H_2O$	$0.4 * 5.3\times10^{-12}$exp(190/T)	
$OH + ROOH \rightarrow RO_2 + H_2O$	1.0×10^{-11}	
Night-time radical formation		
$NO_2 + O_3 \rightarrow NO_3 + O_2$	1.4e-13*exp(-2470/T)	
$NO_3 + NO \rightarrow 2\ NO_2$	2.07e-12*exp(-1400/T)	
$NO_3 + h\nu \rightarrow NO_2 + O$	J-NO_2 × 20.8	
$NO_3 + h\nu \rightarrow NO + O_2$	J-NO_2 × 2.55	
$NO_2 + NO_3 + M \rightarrow N_2O_5 + M$	T and P dependent	

$N_2O_5 + M \rightarrow NO_2 + NO_3 + M$	T and P dependent	
NO_3 + terpenes $\rightarrow$ products	1e-11	
$CH_3C(O)O_2 + CH_3C(O)O_2 \rightarrow 2\ CH_3O_2$	2.9e-12*exp(500/T)	
$CH_3C(O)O_2 + CH_3O_2 \rightarrow HO_2 + CH_3O_2 + HCHO + CO_2$	0.9 * 2.0e-12*exp(500/T)	
$CH_3C(O)O_2 + CH_3O_2 \rightarrow CH_3C(O)OH + HCHO$	0.1 * 2.0e-12*exp(500/T)	

[a] Rate coefficient taken from the IUPAC evaluation. [b]J-O(^{1}D) was modified using water vapour concentrations to take into account relative rates of quenching of O(^{1}D) by air and reaction with H_2O to form 2 OH. [c]Radical channel only (forming H + CHO) [d]As NO, O_3 and NO_2 are all constrained, this reaction has no effect in the model. Parameters constrained by observations were the temperature and pressure as well as mixing ratios of O_3, NO, NO_2, HONO, CO, HCHO, CH_3CHO, terpenes, CH_4 (set to 1.86 ppmv) and dicarbonyls (proportional to HCHO and CH_3CHO). J-values for O_3, HCHO, NO_3, H_2O_2, and the di-carbonyls were based on filter-radiometer measurements.

Box-Model Development

In the following, we describe the stepwise development of the model chemistry (Model 1 to Model 3) and input parameters required to reach the goal of modelling both PAA and H_2O_2. Different simulations within each model are given, for example as M1-S2 (Model 1, Simulation 2). The table below summarises radical production in each model, detailed text concerning each model run is given below.

Table S2. Summary of Models and Simulations

Model	Radical generation and loss	PAA *	H_2O_2 *	HO_2 *[a]	OH *	ROOH *
M1S1	OH reacts only with trace gases constrained by measurement. HO_2: HCHO + *hν*, OH + CO, OH + HCHO, OH + H_2O_2 OH: O_3 + *hν*, H_2O_2 + *hν*, HO_2 + NO, $CH_3C(O)O_2$ + HO_2, terpenes + O_3 $CH_3C(O)O_2$: PAN, OH + CH_3CHO, OH + PAA NO_3 : formation in NO_3 + O_3 and loss by photolysis, reaction with NO, HO_2 and terpenes.	0.20	0.62	0.44	3.4	0.32
M2S1	OH loss rate enhanced OH + OVOC → RO_2 RO_2 + NO → HO_2	0.19	0.47	0.30	0.75	0.25
M2S2	HO*x* recycling (RO_2 + HO_2 → OH)	0.22	0.61	0.36	0.99	0.30
M3S1	$CH_3C(O)O_2$ production increased PAN decomposition rate coefficient increased by factor 5	1.37	0.74	0.43	0.94	2.23
M3S2	$CH_3C(O)O_2$ production rate increased: $CH_3C(O)O_2$ from OH + VOC	0.26	0.42	0.30	0.65	0.35
M3S3	$CH_3C(O)O_2$ and HO_2 from di-carbonyls $CH_3C(O)CHO$ + *hν* → $CH_3C(O)O_2$ + HO_2 BIAC + *hν* → 2 $CH_3C(O)O_2$ HC(O)CHO + *hν* → 2 HO_2 $CH_3C(O)C(O)OH$ + *hν* → $CH_3C(O)O_2$ + HO_2	0.86	1.03	0.49	1.11	1.25

The box-model was constrained by measurements of temperature, O_3, HCHO, CO, NO_2 , PAN, CH_3CHO and J-values. PAA, and H_2O_2 as well as HO*x* were formed photochemically. *Slope of least-squares, linear fit to modelled versus measured mixing ratios. [a]The HO_2 measurements (LIF-HO_2) were heavily biased by detection of RO_2 as described in the manuscript.

M1-S1

In M1-S1, OH production was limited to the photolysis of O_3, HONO and H_2O_2 and the reactions of HO_2 with NO, O_3 and $CH_3C(O)O_2$. HO_2 formation was via photolysis of HCHO and the reactions of OH with CO, HCHO, and H_2O_2 as well as via the reaction of CH_3O (from methane degradation) with O_2. $CH_3C(O)O_2$ was formed from PAN decomposition and in the reactions of OH with CH_3CHO and PAA.

In accord with the observations, the model predicts enhanced PAA and H_2O_2 mixing ratios in the periods impacted by biomass burning, which is related to the increased rate of production of HO_2 (via HCHO photolysis) and $CH_3C(O)O_2$ (via higher levels of CH_3CHO and PAN).

M1-S1 under-predicts PAA on average by a factor of ≈ 5 over the whole campaign. Similarly H_2O_2 is also significantly under-predicted, (on average by a factor of 1.7) though, as for PAA its day-to-day and diel variability are captured reasonably well.

The results of the model calculations are summarised in Table 1. During the campaign, OH was measured (by LIF-FAGE) just above canopy height and at the same height as the PAA/PAN inlets and also at ground level by CIMS). Only the CIMS data set was continuous throughout the campaign as the LIF-FAGE instrument was moved from the ground to the tower following an inter-comparison with the CIMS. Details of the OH measurements are given in Hens et al. (2014) who also show that the higher levels of OH above the canopy are related to a higher actinic flux. On average, the ratio of J-O(^{1}D) above and below the canopy was ≈ 1.9. From Hens et al. (2014), the incremental change in OH (in molecule cm^{-3}) per change in J-O(^{1}D) (in s^{-1}) is roughly given by 1.5×10^{11} OH cm^{-3} s. The difference in measured j-O(^{1}D) above and below the canopy was then used to correct each data-point from the ground-based dataset. The campaign average ratio of OH above to below canopy was 1.55.

Clearly, in M1-S1, the modelled OH concentration, with maximum daytime values as large as 1 x 10^7 molecule cm^{-3} is significantly larger than observed. The overestimation of OH (on average by a factor of 3.4) and the underestimation of HO_2 (and H_2O_2) are due to reactions that convert OH to HO_2 which are not accounted for in M1-S1. Indeed, the model loss rate of OH, obtained by summing over all loss reactions included varies from about 1 to 4 s^{-1}, with a campaign average of 1.3 ± 0.5 s^{-1}, which is much lower than the observed average value of ≈

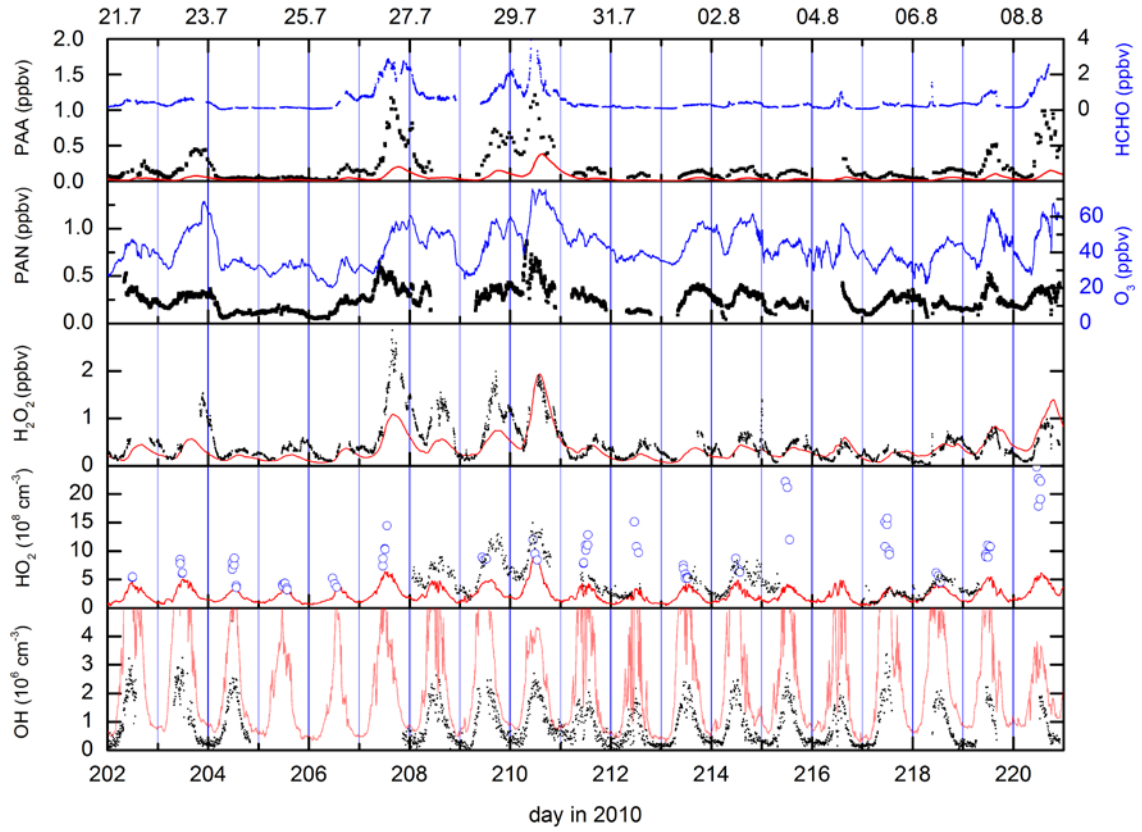

Simulations (in red) from M1S1

12 s^{-1} with a peak reactivity of > 50 s^{-1}, mainly due to reaction with organic trace gases. The difference between model and observation in M1-S1 is expected as the only reactions of OH with organics taken into account are with terpenes, PAA, CH_4 and CH_3CHO.

M2-S1,2

The deviation between modelled and observed OH reactivity was addressed in M2-S1 by adding a generic reaction of OH with oxidised volatile organic trace gases (OVOC) leading to peroxy radicals (RO_2* other than CH_3O_2 and $CH_3C(O)O_2$) which are treated explicitly) and the subsequent formation of HO_2 via their reaction with NO and formation of alkoxy radicals (RO):

$$OH + VOC \rightarrow RO_2^*$$
$$RO_2^* + NO \rightarrow RO + NO_2$$
$$RO + O_2 \rightarrow HO_2 + R'CHO$$

In order to account for the observation that the periods of highest OH reactivity were associated with the biomass burning influenced periods, the modelled concentration of OVOC was tied to that that of HCHO and CH_3CHO. Use of any other short-lived, oxidised organic from the PTRMS dataset would provide a similar variation in OH reactivity (and thus peroxy radical production rates) during the campaign. This is intuitive, as OH reactivity should be correlated with the production of HCHO, an end organic product of the photochemical degradation of many biogenic and anthropogenic trace gases.

Model RO_2^* also reacted with HO_2 to form generic, organic peroxides, ROOH.

$$RO_2^* + HO_2 \rightarrow ROOH + O_2 \qquad (R11)$$

In order to simulate the diel variation of the measured OH loss rates, the concentration of OVOC was set to ~30 times the HCHO or CH_3CHO concentrations with the rate constant for reaction with OH with VOC set to 1×10^{-11} cm^3 $molecule^{-1}$ s^{-1}. The choice of rate coefficient and relative concentration is arbitrary, i.e. a factor 5 lower relative concentration combined with a factor five higher rate coefficient gives the same result.

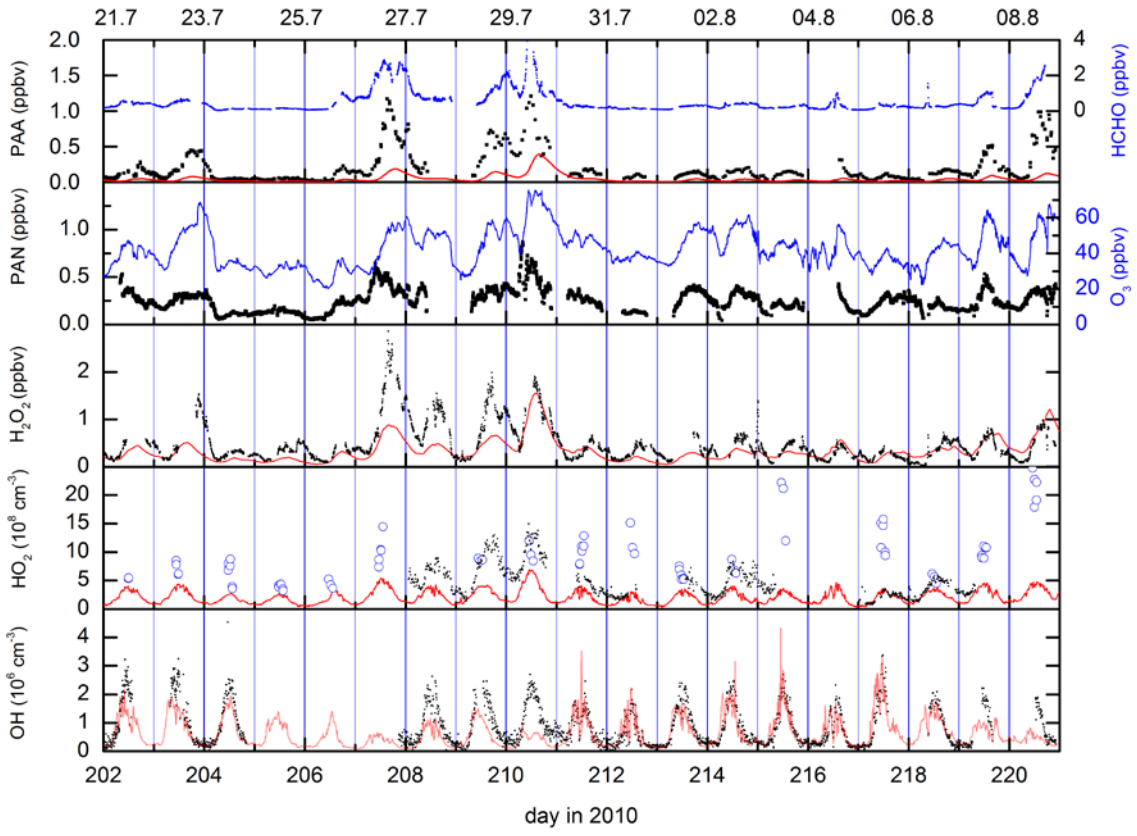

Simulations (in red) from M2S1

This simulation, fails to reproduce the measured PAA, which is underestimated, on average, by a factor ~5. H_2O_2 is also underestimated, though by a smaller amount (on average by a factor ≈ 2). The model underestimates OH slightly (on average by a factor 1.3) but by a factor 2-3 during the biomass-burning influenced episodes. Modelled HO_2, is on average a factor three too low. The model shortcomings are seen most clearly in the biomass-burning episodes, during which the elevated levels of HO*x* and both PAA and H_2O_2 are not reproduced.

As both organic radicals and HO_2 are removed in their mutual reaction (to make ROOH), this reaction was modified (in M2-S2) to force complete radical recycling by generating only OH.

$$RO_2^* + HO_2 \rightarrow OH + \text{products}$$

Whilst, this is known to take place with ~50-60 % efficiency (see above) in the reaction of acetyl peroxy with HO_2, and possibly in reactions of isoprene peroxy radicals with HO_2, in many reactions of organic peroxy radicals with HO_2, the peroxide product dominates (Dillon 2008) so that this represents an upper limit to recycling via this mechanism.

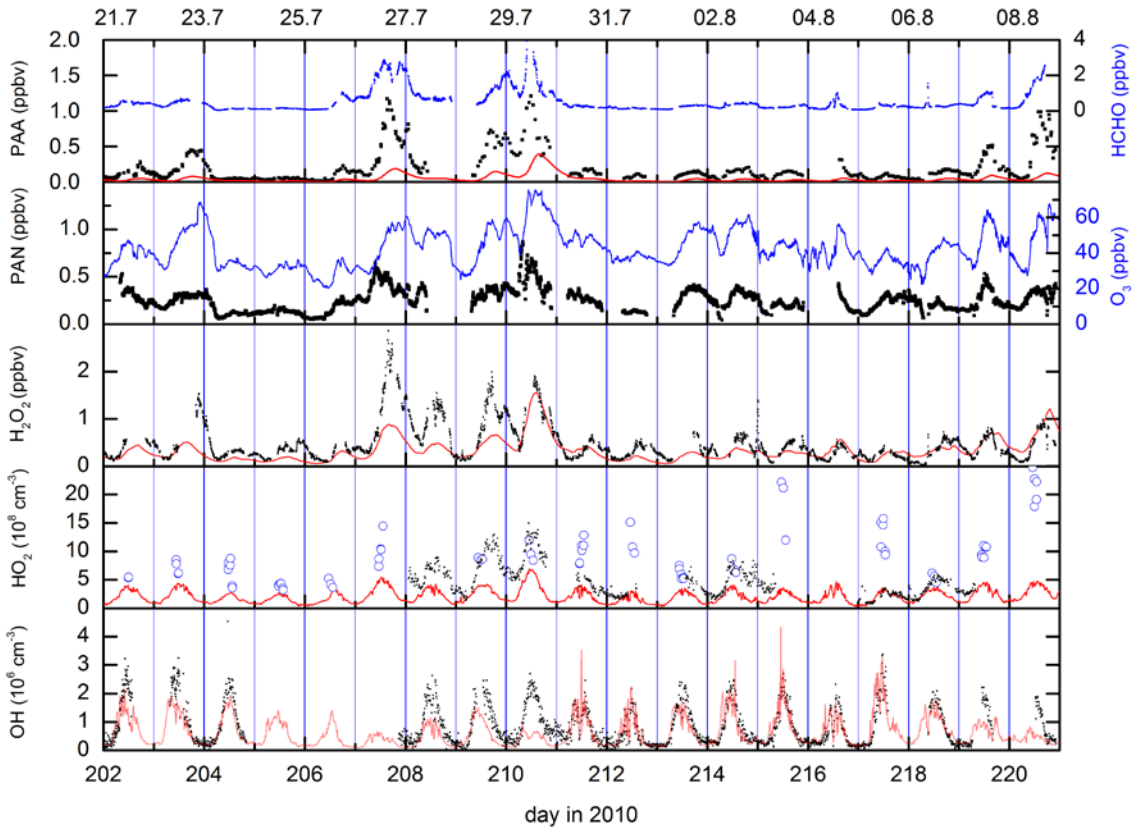

Simulations (in red) from M2S2

Incorporating this reaction in M2-S2 enhanced HO*x* levels only slightly, suggesting that recycling of HO_2 via reaction with NO is in any case dominant. For subsequent model runs, the OH yield from RO_2* + HO_2 was set at 20 %. (i.e. in M3 simulations as discussed below).

The disagreement between modelled and measured H_2O_2 and PAA can have several sources including inaccuracy in the PAA or H_2O_2 measurement, a missing production term for the HO_2 and $CH_3C(O)O_2$ radicals or an overestimation of the deposition velocities. The uncertainty associated with the measurement is estimated at ≈ 30 % (Phillips et al., 2013), which cannot explain the much larger model underestimation. Whilst reduction of the H_2O_2 and PAA deposition velocity has the desired effect of increasing their modelled maximum concentrations it also broadens the diel cycle and modelled H_2O_2 and PAA no longer return to low values ate night-time as observed. We therefore turn to extra chemical sources of radicals to explain the high levels of H_2O_2 and PAA observed compared to the model.

So far, $CH_3C(O)O_2$ production is considered to be via PAN decomposition and reaction of OH with CH_3CHO only. An increase in the PAN decomposition rate would help to increase the concentration of $CH_3C(O)O_2$ and thus, for a given HO_2 level, the PAA formation rate.

M3-S1,2,3

Scenarios in which rates of $CH_3C(O)O_2$ formation were enhanced were tested in M3. Model $CH_3C(O)O_2$ formation can be enhanced by increasing the rate coefficient for PAN decomposition compared to that preferred by the IUPAC and NASA data evaluation panels. In M3-S1, a factor of 5 increase in this parameter was found to result in improved agreement between modelled and measured PAA (slope of 1.37). It also has the desired effect of increasing HO_2 and thus H_2O_2 toward the measured values (slope of 0.74), which stems from reactions of $CH_3C(O)O_2$ with HO_2 and NO forming OH and CH_3O_2, both of which result in enhanced HO*x* production rates. A factor 5 in the PAN decomposition rate constant is however unreasonably large as this parameter is expected to be well determined for the mid-latitude boundary temperatures where most laboratory experimental work on PAN has been conducted. Likewise, increasing the PAN concentration in the model would increase $CH_3C(O)O_2$ production rates, yet the factor required (three-to-five) lie beyond the reported experimental uncertainty for the PAN measurement.

We also simulated (M3-S2) an extra source of $CH_3C(O)O_2$ by adding a fractional production (30 %) of $CH_3C(O)O_2$ formation in the reaction of OH with VOC. Even small increases (less than factor of two) in the modelled concentration of PAA could only be achieved at the cost

of lowering the OH, HO_2 and thus H_2O_2 concentrations significantly, which increases the model-measurement discrepancy.

This is readily understood as PAA is an effective sink of HO*x* for this low NOx environment. A further option to increase the PAA production rate is to introduce a $CH_3C(O)O_2$ production term that does not require initiation by reaction with OH, i.e. photolysis of a precursor trace gas, essentially an oxidised organic which results in CH_3CO release. This is described in detail in the main manuscript.

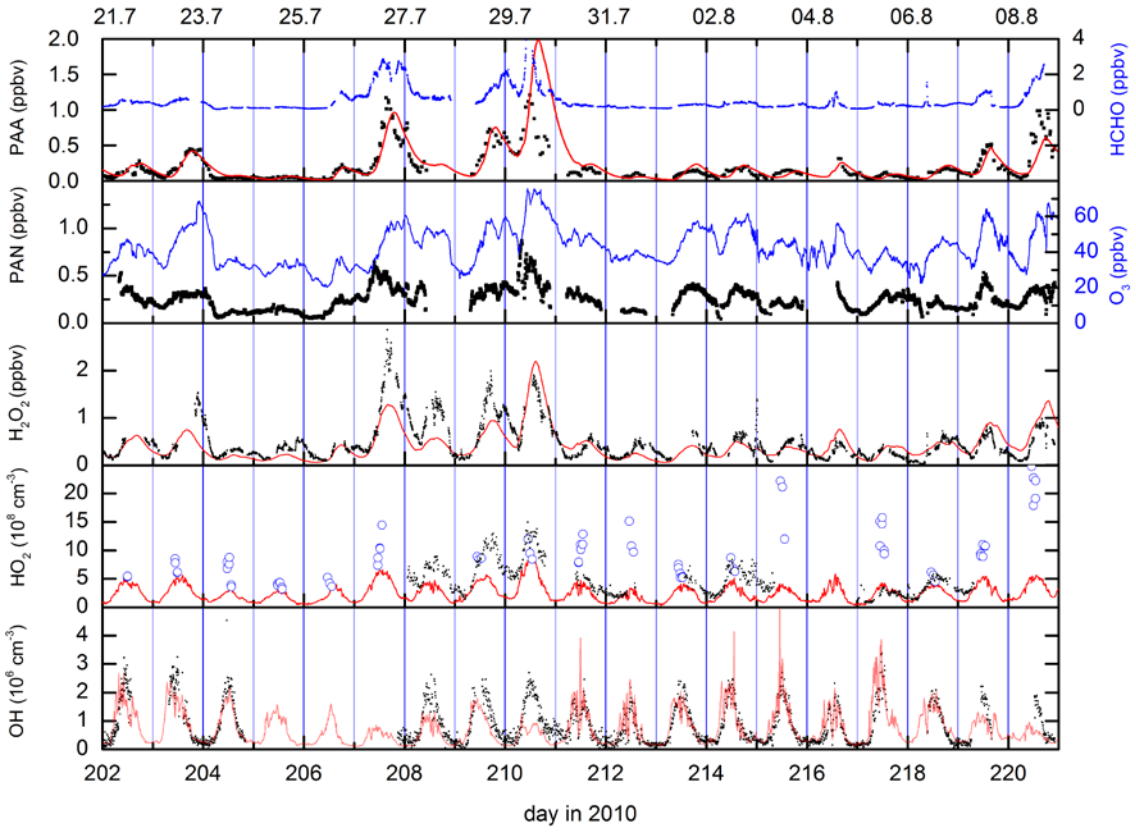

Simulations (in red) from M3S1

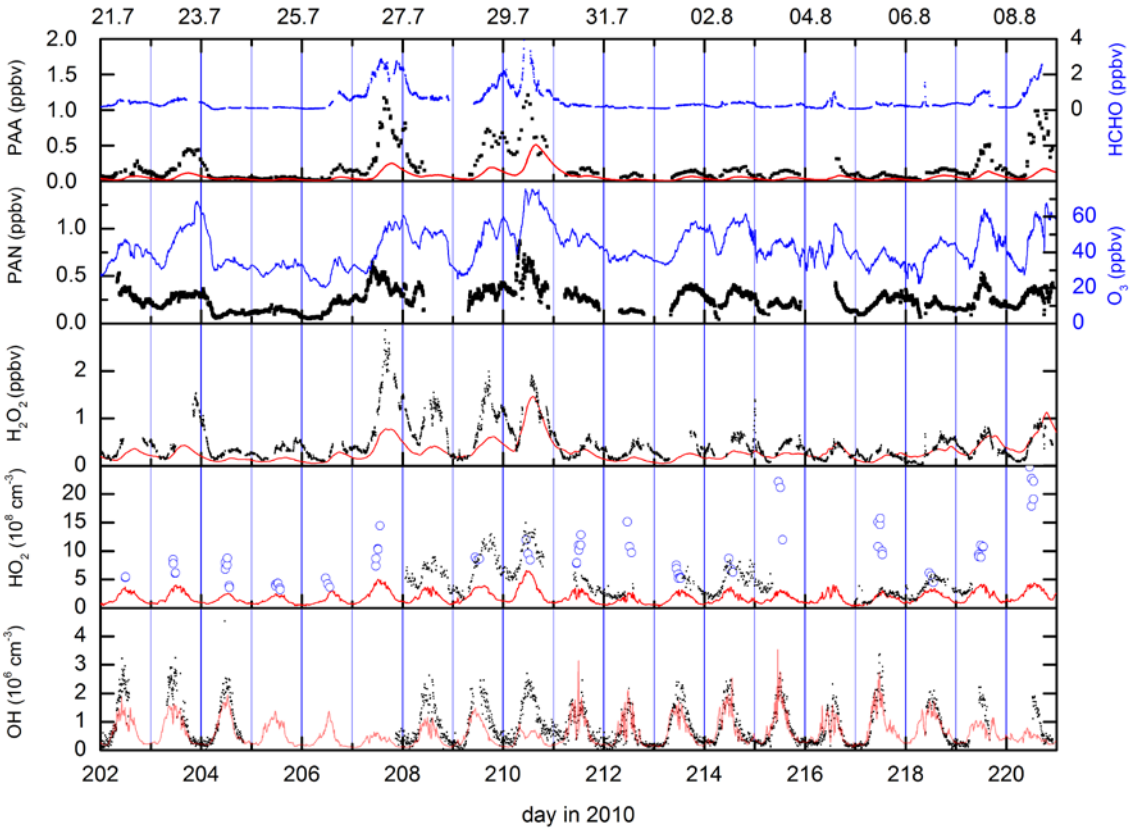

Simulations (in red) from M3S2

References

Hens, K., Novelli, A., Martinez, M., Auld, J., Axinte, R., Bohn, B., Fischer, H., Keronen, P., Kubistin, D., Nolscher, A. C., Oswald, R., Paasonen, P., Petaja, T., Regelin, E., Sander, R., Sinha, V., Sipila, M., Taraborrelli, D., Ernest, C. T., Williams, J., Lelieveld, J., and Harder, H.: Observation and modelling of HOx radicals in a boreal forest, Atmos. Chem. Phys., 14, 8723-8747, doi:10.5194/acp-14-8723-2014, 2014.

Phillips, G. J., Pouvesle, N., Thieser, J., Schuster, G., Axinte, R., Fischer, H., Williams, J., Lelieveld, J., and Crowley, J. N.: Peroxyacetyl nitrate (PAN) and peroxyacetic acid (PAA) measurements by iodide chemical ionisation mass spectrometry: first analysis of results in the boreal forest and implications for the measurement of PAN fluxes, Atmos. Chem. Phys., 13, 1129-1139, doi:doi:10.5194/acp-13-1129-2013, 2013.